Chemistry–A European Journal
Research Article
doi.org/10.1002/chem.202201792
Chemistry Europe
European Chemical Societies Publishing
www.chemeurj.org

Catalysis by $[Ga_4L_6]^{12-}$ Metallocage on the Nazarov Cyclization: The Basicity of Complexed Alcohol is Key

Gantulga Norjmaa,[a] Fahmi Himo,[b] Jean-Didier Maréchal,[a] and Gregori Ujaque*[a]

Abstract: The Nazarov cyclization is investigated in solution and within $K_{12}[Ga_4L_6]$ supramolecular organometallic cage by means of computational methods. The reaction needs acidic condition in solution but works at neutral pH in the presence of the metallocage. The reaction steps for the process are analogous in both media: (a) protonation of the alcohol group, (b) water loss and (c) cyclization. The relative Gibbs energies of all the steps are affected by changing the environment from solvent to the metallocage. The first step in the mechanism, the alcohol protonation, turns out to be the most critical one for the acceleration of the reaction inside the metallocage. In order to calculate the relative stability of protonated alcohol inside the cavity, we propose a computational scheme for the calculation of basicity for species inside cavities and can be of general use. These results are in excellent agreement with the experiments, identifying key steps of catalysis and providing an in-depth understanding of the impact of the metallocage on all the reaction steps.

Introduction

Supramolecular chemistry is an interdisciplinary field with a spectrum of applications that ranges from molecular recognition to catalysis.[1,2] This field shares numerous similarities with processes observed in enzymes, the most striking one is the importance host-guest interactions in dictating both the binding process of the guest and controlling the catalytic profiles.[1,2] This parallelism between host-guest and receptor-ligand of biomacromolecules has been largely pursued by chemists to make efficient cages.

A range of synthetic hosts has been designed and optimized enriching the toolbox of available supramolecules. Amongst them, the so-called metallocages, Supramolecular Organometallic Complexes (SOCs) or Metal–Organic Cages (MOCs) are among of the most exciting ones. These are obtained by self-assembly of metal ions or clusters with organic ligands and the final structure are mainly driven by coordination rules.[3] This strategy gives rise to a great diversity of well-defined topologies at the nanoscale that could not be reached with pure organic scaffolds. Their internal cavities are attractive for hosting molecules with high selectivity and specificity, with many applications,[4–6] including catalysis.[7–9] Many metallocages have been employed as supramolecular catalysts[9–13] including Raymond's[14] Ga_4L_6, Fujita's[15] Pd_6L_4, Nitschke's[16] Fe_4L_6, or Lusby's Pd_2L_4 among others.[17]

The tetrahedron host $K_{12}[Ga_4L_6]$ designed by Raymond and coworkers has been demonstrated to accelerate several chemical reactions, such as the hydrolysis of orthoformates,[18] reductive elimination from Au(III) and Pt(IV) complexes,[19–23] hydroalkylation,[24] allyl alcohol isomerization,[25] and aza-Cope rearrangement,[26] among others.[27,28] The Nazarov cyclization (Scheme 1a), the subject of the present investigation, is a very useful reaction for the formation of cyclic compounds by means of C–C bond forming process and has also been demonstrated to be catalyzed by the $K_{12}[Ga_4L_6]$ metallocage.[29]

Under common reaction conditions, the Narazov cyclization requires acidic media to proceed. However, in the presence of metallocage $[Ga_4L_6]^{12-}$, **3**, the process can take place at pH 8 (Scheme 1a). The rate acceleration is ca. 10^6 times (Scheme 1b), reaching a degree of rate acceleration comparable to those observed in several enzymes.[30] The increase in reaction rate was initially attributed to a combination of several factors, such as (a) preorganization of the encapsulated substrate, (b) transition state stabilization of the cyclization by constrictive binding, and (c) increase of the basicity of the complexed alcohol functionality. A subsequent mechanistic study by Raymond and coworkers showed that the electrocyclization is the rate-determining step for the uncatalyzed reaction, while the electrocyclization and the water loss from the substrate are both rate-determining for the cage-catalyzed reaction.[31] Moreover, according to their mechanistic analysis, transition state

[a] *Dr. G. Norjmaa, Dr. J.-D. Maréchal, Dr. G. Ujaque*
Departament de Química and Centro de Innovación en Química Avanzada (ORFEO-CINQA)
Universitat Autònoma de Barcelona
08193 Cerdanyola del Valles, Barcelona, Catalonia (Spain)
E-mail: jeandidier.marechal@uab.cat
gregori.ujaque@uab.cat

[b] *Prof. Dr. F. Himo*
Department of Organic Chemistry, Arrhenius Laboratory, Stockholm University
10691, Stockholm (Sweden)
E-mail: fahmi.himo@su.se

Supporting information for this article is available on the WWW under https://doi.org/10.1002/chem.202201792

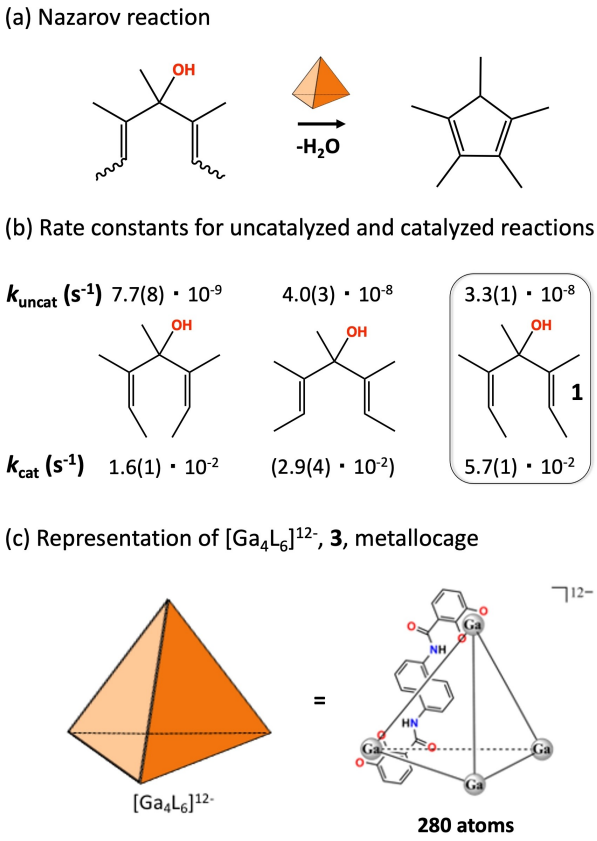

Scheme 1. (a) Nazarov cyclization in presence of metallocage **3**. (b) Experimental rate constants obtained for three different substrates; the highlighted one has been selected for this study. Rate constants from Ref. [29] and [31]. (c) Schematic representation of the $[Ga_4L_6]^{12-}$ metallocage, **3**.

stabilization of the cyclization was found to significantly contribute to the dramatic rate enhancement.[31]

Computational chemistry has become an indispensable tool in the study of reaction mechanisms. It provides detailed understanding of the processes that is not easily accessible by experimental techniques. In the case of supramolecular catalysis, computational methods have only been applied recently mainly because of the large dimensions of the systems.[21–23,32–44]

In the current contribution, we present a computational study with the aim of identifying the factors causing the rate enhancement of the Nazarov reaction inside the metallocage as compared to solution. We use a combination of quantum mechanical (QM) calculations and molecular dynamics (MD) simulations, and the overall description of the reaction mechanism is obtained by connecting experimental and computational results to describe the reaction steps for the process. Overall, computational results are in excellent agreement with experiment and provide a deeper understanding of the process identifying the key aspects of catalysis. While this manuscript was under review appeared a publication by Tantillo, Toste, Bergman, Raymond and coworkers on the same topic reaching essentially the same conclusions about the origin of catalysis.[45]

Results and Discussion

The Nazarov cyclization was experimentally investigated for three related 1,4-pentadien-3-ols substrates (Scheme 1b). Because the asymmetric compound **1** shows the highest rate constant for the catalyzed reaction and yields no unexpected product (dihydrofulvene isomer), it was selected as case system.

A general schematic representation of the most important intermediate structures for the mechanism are illustrated in Scheme 2 (black arrows for the uncatalyzed reaction and orange arrows for the catalyzed one).[29,31] The main steps for the cyclization process can be described as: (i) protonation of the alcohol group of the substrate, **2**, (ii) water loss from the substrate, forming a carbocationic species, **4**, and (iii) formation of the five-membered ring, **5**, by electrocyclization.

In what follows, we will present the computational analysis of the reaction mechanism in solution first, followed by the reaction inside the metallocage, step by step, involving encapsulation, protonation, water loss and cyclization.

Reaction in Solution

The equilibrium between substrate **1**, with an alcohol group, and its protonated form **2**, depends on the pH of the solution. The reaction requires acidic pH in the absence of the metallocage **3**, whereas in its presence it can be performed at pH 8. The energy of the protonated reactant can be obtained from the pK_a of protonated species **2**, which under the reaction conditions in the presence of the cage (pH 8.0 and 45 °C) was experimentally estimated to be −5.0.[31] Therefore, the energy of the protonated 1,3-pentadienol substrate **2** was estimated by Raymond and coworkers to be 18.9 kcal/mol higher than the neutral substrate **1**.[31]

Computing relative Gibbs energy values for protonated vs. non-protonated species corresponds to the calculation of the pK_a of the protonated alcohol.[46] Following a standard procedure for the calculation of pK_a values,[46,47] we determined the Gibbs energy difference between protonated and non-protonated states to be 19.5 kcal/mol, in excellent agreement with the experimentally estimated value. The procedure to compute pKa is by calculating the standard Gibbs energy of deprotonation (ΔGs(deprot)) of the protonated alcohol in gas phase along with the Gibbs energy of solvation of all the species involved in the thermodynamic cycle: ROH_2^+, $(H_2O)_n$, ROH and $H_3O^+(H_2O)_{n-1}$ (see Scheme S1 in the Supporting Information). It is important to point out that in order to obtain this Gibbs energy we evaluated how the number of explicit water molecules considered in the model affects the results. Thus, the Gibbs energy difference (ΔG) between the neutral substrate, **1**, and the protonated form, **2**, were calculated including one (**1-w1** vs. **2-w1**), two (**1-w2** vs. **2-w2**), three (**1-w3** vs. **2-w3**), or four explicit water molecules (**1-w4** vs.**2-w4**). The results clearly show that the energies converge at 3 explicit water molecules (Figure S1 and Table S2). Calculations inside the metallocage will be also done including 3 water molecules; MD simulations of the protonated substrate show that an average of 3 water

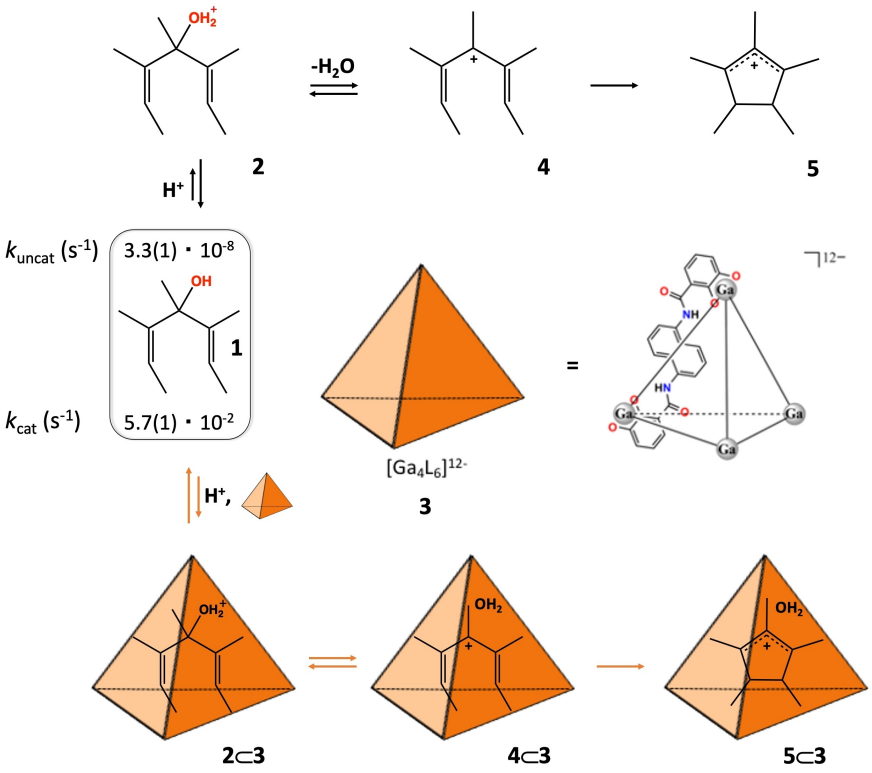

Scheme 2. General schematic representation of the Nazarov cyclization of 1,4-pentadien-3-ol, **1**, in solution and in the metallocage. Rate constants are taken from Ref. [29].

molecules are inside the metallocage (see below). In both systems, solution and inside the metallocage, 3 water molecules need to be explicitly considered in the model.

We thus selected **2-w3** as starting model of the protonated substrate for the reaction in solution. A conformational analysis of **2** shows that the most stable conformation is the one named "open" in Figure 1, whereas the reactive conformation, named "closed", is calculated to be only 0.5 kcal/mol higher in energy, showing that it is highly accessible. When three explicit solvents molecules are included in the calculations, the difference between open (the most stable) and closed one is 0.3 kcal/mol. Energies of other conformations are given in the Supporting Information (Table S1).

After the protonation, the next step in the reaction is the water loss from the protonated substrate. This was calculated to have a barrier of 7.1 kcal/mol relative to **2-w3**, which is 26.6 kcal/mol relative to the global zero (Figure 3), and the following intermediate, **4-w3**, is 5.3 kcal/mol higher than the **2-w3** (+24.8 kcal/mol relative to the zero). At the transition state, $\mathbf{TS_{2\text{-}w3}}$, the $\mathbf{d_{C\text{-}Ow}}$ distance is elongated to 2.37 Å (Figure 2). From **4-w3** the electrocyclization takes place through $\mathbf{TS_{4\text{-}w3}}$, calculated to have an energy of 29.9 kcal/mol (Figure 3). This is the rate-determining step of the reaction, in agreement with the experimental value of 30.0 kcal/mol, obtained from the measured rate constant of $3.3 \cdot 10^{-8}\ s^{-1}$ at 45 °C.[29,31] Moreover, the difference between two calculated barriers, 26.6 kcal/mol for water loss and 29.9 kcal/mol for electrocyclization, is also in good agreement with experimental observations of the latter step as the rate determining step.

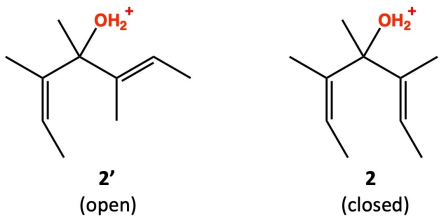

Figure 1. Open (**2'**) and closed (**2**) conformers of the protonated substrate.

Reaction in metallocage: Encapsulation and protonation of substrate

The Gibbs energy associated to the encapsulation of alcohol **1** was experimentally determined to be 0.3 kcal/mol ($\Delta G_{4,exp.}$). It is expected that under reaction conditions all the metallocages are occupied with the substrate (the concentration of the reactant is much larger than that of the metallocages). The encapsulation process was calculated using a protocol we recently established[48] for calculating binding Gibbs energies in supramolecular metallocages using the attach–pull–release (APR) method (see computational details). This protocol showed good agreement between calculated and experimental binding Gibbs energies for a set of cationic guests encapsulated in the

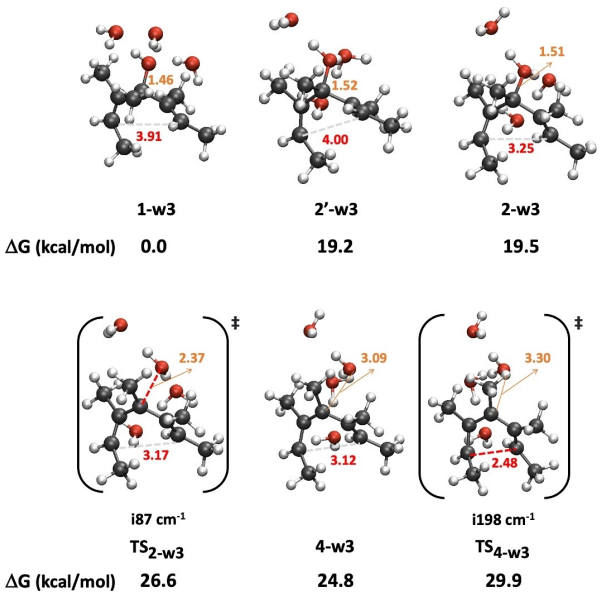

Figure 2. Geometries of intermediates and TSs for the reaction in solution. Distances are in Å; Gibbs energies in kcal/mol; imaginary frequencies in cm^{-1}.

$[Ga_4L_6]^{12-}$ metallocage. Its application to substrate **1** gives a Gibbs binding energy ($\Delta G_{4,calc.}$) of 3.2 kcal/mol, in fairly good agreement with experiment.

Once encapsulated, the next step in the reaction is the protonation of the substrate. Direct computation of Gibbs energy for this protonation step is not affordable: it implies calculating the pK_a of the protonated substrate inside the metallocage. The general thermodynamic cycle employed to calculate pKa cannot be utilized here to accurately determine the Gibbs energy for the protonation of the substrate within the metallocage; such a cycle needs the value of the Gibbs energy for the solvation of the encapsulated proton (from the gas phase to solution). Nevertheless, the calculation of this magnitude is not reliable using continuum methods.[46] Instead, the Gibbs energy difference between protonated and non-protonated substrate inside the metallocage (ΔG_3) can be obtained using an alternative thermodynamic cycle, as the one shown in Figure 4. According to this, the relationship between the Gibbs energies for protonating the neutral substrate (in both, solution, ΔG_2, and inside metallocage, ΔG_3), must be the same than the relationship between the Gibbs energies of encapsulating both, the neutral, ΔG_4, and protonated, ΔG_1, substrates. For two of the steps of the thermodynamic cycle the Gibbs energy can be estimated, $\Delta G_{2,est}$ and experimentally obtained, $\Delta G_{4,exp}$. $\Delta G_{1,calc}$ and $\Delta G_{4,calc}$, corresponding to the binding of the neutral and protonated substrate in the metallocage, are computed using the APR method based on molecular dynamics simulations. $\Delta G_{2,calc}$, in turn, which corresponds to the protonation of neutral substrate in solution, is calculated at DFT level. In Figure 4 are shown all computed Gibbs energies (in blue) and experimental and estimated values (in green). The computed values are in excellent agreement with experiment:

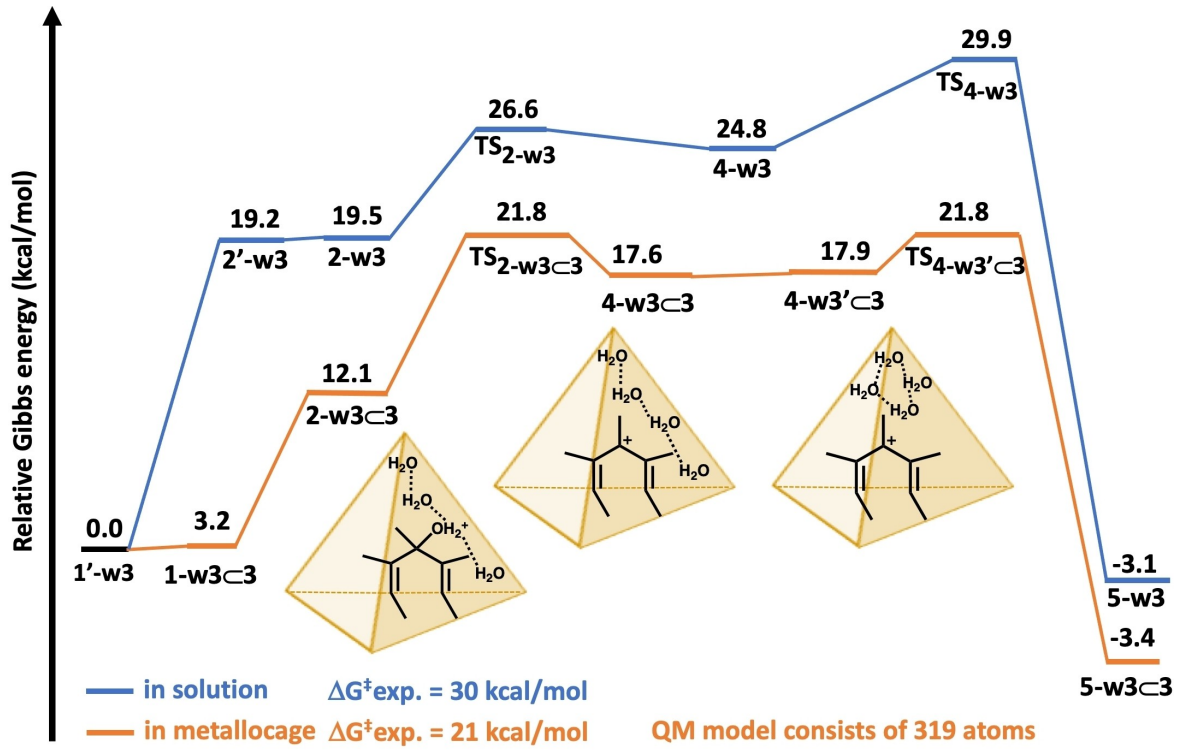

Figure 3. Calculated Gibbs energy reaction profile for the Nazarov cyclization in solution and in the presence of metallocage **3**.

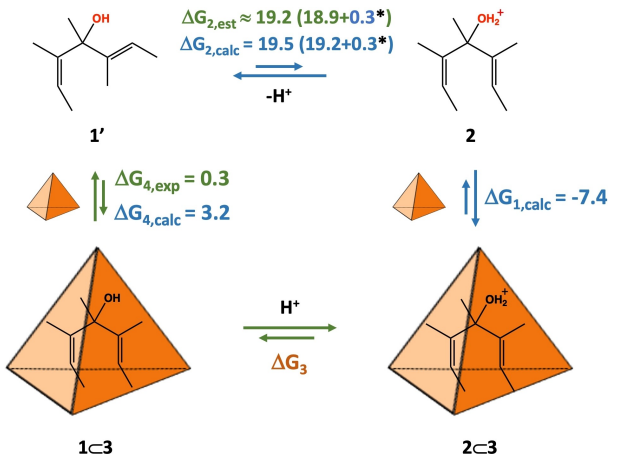

Figure 4. Thermodynamic cycle to obtain the basicity (ΔG_3) of the encapsulated reactant **1**. (*) "closed" conformation of the protonated substrate is 0.3 kcal/mol higher in Gibbs energy than the most stable one. Gibbs energies in kcal/mol.

$\Delta G_{2,est} = 19.2$ vs. $\Delta G_{2,calc} = 19.5$ kcal/mol, and $\Delta G_{4,exp} = 0.3$ vs. $\Delta G_{4,calc} = 3.2$ kcal/mol, respectively. The encapsulation of the protonated alcohol, **2**, to the metallocage, ΔG_1, cannot be determined experimentally. Nevertheless, the binding energy for this process can be obtained using the protocol previously commented.[48] The calculation gives a binding Gibbs energy for this process, $\Delta G_{1,calc}$, of −7.4 kcal/mol. Encapsulating the protonated substrate would be an exergonic process (Figure S2).

In the thermodynamic cycle (Figure 4), the values of the Gibbs energies are $\Delta G_{2,calc} = 19.5$ kcal/mol, $\Delta G_{4,calc} = 3.2$ kcal/mol and $\Delta G_{1,calc} = -7.4$ kcal/mol. Assuming that these ΔG values can be combined despite being obtained by means of different computational approaches, the calculated Gibbs energy for the protonation of the encapsulated neutral substrate, ΔG_3 is 8.9 kcal/mol. According to this, the encapsulated protonated substrate, (**2-w3⊂3**), has a relative Gibbs energy of 12.1 kcal/mol within the reaction profile (Figure 3).

The Gibbs energies associated to these protonation steps in solution and inside the metallocage are 19.5 kcal/mol for **2-w3** and 12.1 kcal/mol for **2-w3⊂3**, respectively (Figure 3). The comparison of these values reveals that the protonation process is much more accessible inside the cage than in solution by 7.4 kcal/mol. In a related study, Warshel and coworkers[38] also found that the rate acceleration by the same $[Ga_4L_6]^{12-}$ metallocage on a related process, hydrolysis of orthoformate, is mainly due to large stabilization of H_3O^+ inside the metallocage (pointing out a very low "local pH") and the electrostatic stabilization of the positively charged transition state. Similarly, the dramatic change of basicity of the alcohol over encapsulation observed here is crucial for accelerating the reaction. In fact, accessing to the **2-w3⊂3** intermediate takes place at the beginning of the process, thus all the reaction steps taking place afterwards are largely affected. The Gibbs energy difference for this protonation step in solution and inside the metallocage has the largest impact on the overall reaction.

To analyze the effect of the metallocage on the conformation, the Gibbs energy of encapsulation for the open and closed conformations of the protonated substrate were calculated employing the above-mentioned protocol.[48] The values obtained are −5.4 kcal/mol and −7.4 kcal/mol, for open and closed conformations, respectively, showing that the closed conformation is favored by 2.0 kcal/mol.

The analysis was complemented by performing a classical molecular dynamic (MD) simulation of the encapsulated protonated substrate in a periodic box of explicit solvents (see computational details) and additional DFT calculations. The MD simulations show that there is an average of two to three solvent water molecules around the protonated substrate within the metallocage (see Figure S3). For computing the relative Gibbs energies at DFT level we considered a model with 3 solvent molecules encapsulated. To identify the most stable situation of the encapsulated system, different arrangements (molecular conformations, water disposition) selected from the most populated structures along the MD were fully optimized at DFT level. Interestingly, the closed conformation (the reactive one) is calculated to be the most stable one, **2-w3⊂3** by 4.2 kcal/mol compared to the lowest open conformation arrangement, **2'-w3⊂3**. This confirms that the energy difference between encapsulated open and closed conformations favors the latter by ~2-4 kcal/mol (note that in solution both conformations were very similar in energy). Hence, encapsulation induces the proper preorganization of the substrate, making the closed conformation the most stable one inside the metallocage thus facilitating the reaction.

Reaction in metallocage: Water loss

To obtain an accurate reaction profile within the metallocage at DFT level one needs to properly describe the behavior of encapsulated protonated substrate, thus including the locally surrounding solvent molecules. In the previous section we presented classical molecular dynamic (MD) simulations of the encapsulated protonated substrate in a periodic box of explicit solvents. The simulations indicate that there are around three solvent water molecules along with the protonated substrate within the metallocage (see Figure S3). Thus, for calculating the Gibbs energy profile at DFT level we selected the most stable structure, **2-w3⊂3**, which includes the protonated substrate on the closed conformation and three water molecules altogether in the $[Ga_4L_6]^{12-}$ metallocage.

The optimized geometries of intermediates and transition states for encapsulated substrate along with three explicit water molecules are shown in Figure 5. The encapsulated protonated intermediate, **2-w3⊂3**, as previously shown, has an estimated relative Gibbs energy of 12.1 kcal/mol within the reaction profile (Figure 3). The transition state for the water loss from the protonated substrate inside the metallocage, $\mathbf{TS_{2\text{-}w3\subset3}}$, has a relative Gibbs energy barrier of 9.7 kcal/mol, with a global barrier of 21.8 kcal/mol. The distance of the protonated alcohol C–O bond ($\mathbf{d_{C\text{-}Ow}}$) is elongated to 2. 37 Å at the transition state ($\mathbf{TS_{2\text{-}w3\subset3}}$) from 1.51 Å at the intermediate (**2-w3⊂3**).

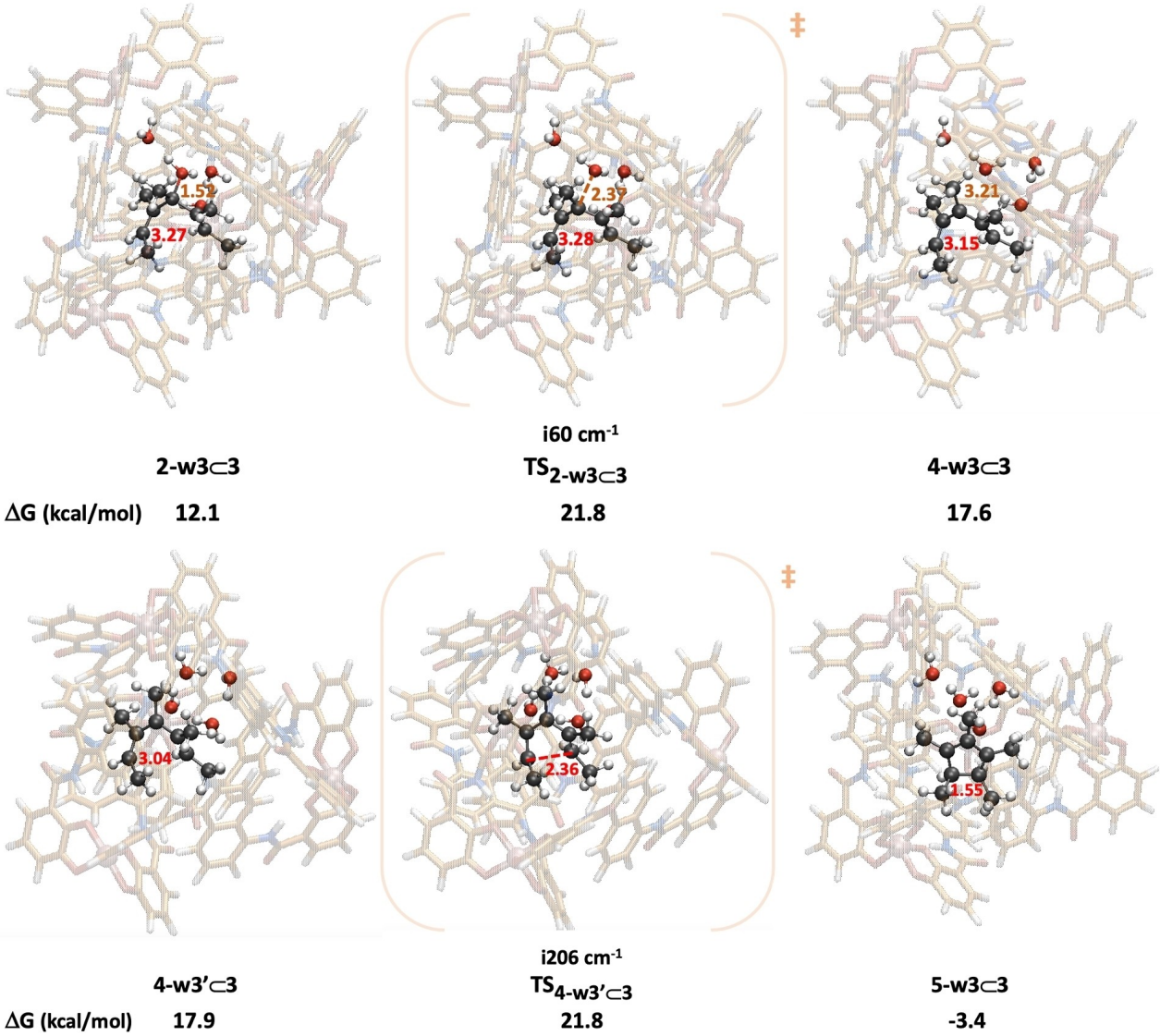

Figure 5. Optimized geometries and relative Gibbs energies for the intermediates and TSs of the Nazarov cyclization inside metallocage **3**; imaginary frequencies in cm^{-1}.

Once the substrate is protonated, next step in the process corresponds to water loss. The Gibbs energy barrier for this process in solution (from **2-w3** to $\mathbf{TS_{2\text{-}w3}}$) is 7.1 kcal/mol, whereas the analogous step inside the metallocage is 9.7 kcal/mol (from **2-w3⊂3** to $\mathbf{TS_{2\text{-}w3}}$⊂**3**). Therefore, performing the process inside the metallocage provokes an increase of the barrier of 2.7 kcal/mol for this step. Water loss inside the cavity leads to a penalty in terms of Gibbs energy barrier, although that penalty is not large. Such an increase on the Gibbs energy barrier is somewhat relevant because involves that this step becomes rate limiting along with the cyclization (see below).

At this point it is worth commenting how is affected the Gibbs energy barrier for the reversal process of water loss in solution (water addition from intermediate **4-w3**) and inside the metallocage (**4-w3⊂3**). In solution, the relative Gibbs energy barrier (from **4-w3** to $\mathbf{TS_{2\text{-}w3}}$) is 1.8 kcal/mol, whereas the corresponding barrier inside the metallocage (from **4-w3⊂3** to $\mathbf{TS_{2\text{-}w3}}$⊂**3**) is 4.2 kcal/mol. This is in very good agreement with experiment where it has been shown that the backward reaction step inside the metallocage is more energy demanding than in solution.[29,31] Altogether, the effect of the metallocage on the water loss step, despite non favoring the process, is relatively moderate.

Reaction in metallocage: Cyclization

Before analyzing the cyclization step, we investigated the accessibility for a conformational change of **4** inside the metallocage; a modification from closed to other open conformation should be highly detrimental for the reaction. To that purpose, we performed an Adaptively Biased Molecular Dynam-

ic (ABMD) simulation with AMBER 16 program using two torsion angles as collective variables (see Figure S5). The simulation shows that the conformational change within the metallocage is too energetically demanding to be affordable (more than 20 kcal/mol). Thus, the closed conformation is maintained once the intermediate after water loss is formed.

The encapsulated intermediate after the water loss, **4-w3⊂3**, is calculated to be at 17.6 kcal/mol in Gibbs energy relative to **1**. For the next step, cyclization, the lowest energy barrier step was found with a different arrangement of the water molecules inside the cavity, **4-w3'⊂3**. The calculations show that the relative Gibbs energy of this intermediate is not significantly affected by the solvent rearrangement inside the metallocage; the calculated relative Gibbs energies are 17.6 and 17.9 kcal/mol for **4-w3⊂3** and **4-w3'⊂3**, respectively. These rearrangements of water molecules in the metallocage are schematically illustrated in Figure 3 and their optimized geometries are shown in Figure 5. For the cyclization process itself, several transition states with different molecular arrangements were optimized. The lowest energy one, $\mathbf{TS_{4\text{-}w3'\subset 3}}$, is 3.9 kcal/mol above **4-w3'⊂3**, located at 21.8 kcal/mol from **1**, (Figure 3). The optimized geometries of the transition state with different rearrangements of water solvent molecules in the metallocage are shown in the Supporting Information (Figure S4b). Such water arrangements have larger effect on the Gibbs energy of the transition states than on the intermediates (**4-w3⊂3** and **4-w3'⊂3** in Figure 3). These two intermediates, species **4-w3⊂3** and **4-w3'⊂3** are very similar in energy, just involving a solvent reorganization. The forming C–C bond distance at this transition state is 2.364 Å (Figure 5). The formation of the cyclic carbocationic intermediate, **5-w3⊂3**, is highly exergonic with a Gibbs energy of −3.4 kcal/mol. Therefore, the reaction is irreversible once the cyclized species is formed.

To evaluate the magnitude of the stabilization of the cyclization TS associated to the encapsulation, one needs to compute and compare its barrier in solution and inside the metallocage. The relative Gibbs energy barrier associated to this step in solution is 5.1 kcal/mol (from **4-w3** to $\mathbf{TS_{4\text{-}w3}}$), whereas that for the cyclization step inside the metallocage is 3.9 kcal/mol (from **4-w3'⊂3** to $\mathbf{TS_{4\text{-}w3'\subset 3}}$); the energy barrier decreases by 1.2 kcal/mol. Thus, despite the metallocage favors the cyclization step, the effect on the overall process is relatively moderate.

The increase of the Gibbs barrier for the water loss along with the fact that the relative Gibbs energy barrier for the electrocyclization diminishes inside the metallocage, involves that the relative Gibbs energy value for the transition states of water loss ($\mathbf{TS_{2\text{-}w3\subset 3}}$) and cyclization ($\mathbf{TS_{4\text{-}w3'\subset 3}}$) acquire both the same value of 21.8 kcal/mol. Therefore, both steps are involved in defining the reaction rate of the process, once again in very good agreement with experiment.[31] Moreover, the calculated Gibbs energy barrier of 21.8 kcal/mol for both rate determining steps is also in excellent agreement with the estimated value of 21.0 kcal/mol (from the experimental rate constant of $5.7 \cdot 10^{-2}$ s^{-1} at 45 °C).

Conclusions

The reaction mechanism for the Nazarov cyclization was analyzed in solution and inside the $[Ga_4L_6]^{12-}$ metallocage by means of computational methods combining DFT and classical molecular dynamics calculations.

The reaction mechanism in solution and inside metallocage have the same reaction steps: (i) protonation of the alcohol group of the substrate (ii) water loss from the substrate, forming a carbo-cationic species, and (iii) formation of the five-member ring, **5**, by electrocyclization. Nevertheless, upon encapsulation the Gibbs energy profile is dramatically affected.

The first step in the reaction is the protonation of the substrate. The associated Gibbs energies in solution and inside the metallocage are 19.5 kcal/mol for ΔG_2 and 12.1 kcal/mol for ΔG_3, respectively (Figure 4). The comparison of these values reveals that the protonation process is much more accessible inside the cage than in solution by 7.4 kcal/mol. This becomes the most important factor for accelerating the reaction rate.

Additionally, whereas in solution an open conformation is favored (too far from the catalytically competent geometry for cyclization), inside the metallocage a closed conformation with a geometry close to the reactive form is preferred (by 2 to 4 kcal/mol, depending on the method employed). Therefore, the metallocage promotes a preorganization of the substrate for the reaction to proceed.

The next step, the water loss, pays a penalty in terms of Gibbs energy barrier inside the cavity, although the effect is quite moderate. Its Gibbs energy barrier is 7.1 kcal/mol in solution and 9.7 kcal/mol once encapsulated. Such a relative increase in the barrier involves that this step also becomes rate limiting along with the cyclization. Finally, the Gibbs energy barrier of the cyclization is lowered when occurring inside the cage by 1.2 kcal/mol. It suggests a relatively moderate effect of the supramolecular host on the rate acceleration regarding the cyclization step.

Overall, despite preorganization of the substrate upon encapsulation helps the process, the ability of the metallocage to stabilize the cationic species (protonated alcohol) is the crucial factor for the rate acceleration observed. The ensuing two steps, water loss and cyclization, are both affected moderately by encapsulation. Understanding and evaluating these effects should help to the rational design of novel host-guest catalyses.

Computational Details

All DFT calculations were performed using the Gaussian 09 software[49] with the B3LYP–D3 functional.[50–52] The SDD pseudopotential and related basis set, complemented with a set of d polarization functions, were used for Ga,[53,54] while the 6-31G(d) basis set was used for all other atoms.[55] The structures of the reactants, intermediates, transition states and products were optimized in water solvent by using the SMD continuum model. [56] These calculations involve systems with more than 300 atoms. The quasi-rigid-rotor-harmonic-oscillator (quasi-RRHO) approach was used for thermal contributions to the Gibbs energies.[57] The standard state correction (1.9 kcal/mol to each of the compounds)

was also included. [58] Gibbs energies were calculated at full DFT level except the binding of the neutral and protonated substrate in the metallocage which were computed using the APR method (see below).

MD simulations were performed with the AMBER 16 package[59] using the CUDA version of the pmemd program. The MD simulation box, of size 46×49×47 Å and treated under periodic boundary conditions, contains the metallocage, the guest, 11 potassium counterions, and ~2500 water molecules (TIP3P). [60] The simulations were performed at constant temperature (298.15 K, using a Langevin thermostat) and pressure (1 bar, using a Monte Carlo barostat). Force field parametrization procedure was described in our previous work (the parameters of the metallocage were directly used). [48] The absolute binding Gibbs energies (ΔG_{bind}) were computed using the attach–pull–release (APR) method.[61–63] The simulation details were described in the previous work [48] and can be summarized as: (i) derivation of non-standard parameters needed for the host and guest molecules, (ii) combining the derived parameters with the general AMBER force field, (iii) calculating the binding Gibbs energy with the APR method. The adaptively biased molecular dynamics (ABMD) [64] simulations were performed to analyze the conformational change of the carbocationic intermediate inside the metallocage (see Supporting Information and Figure S5).

Acknowledgements

We thank D. Tantillo and coworkers for generously sharing results before publication (their work appeared in Ref. [45]). The authors acknowledge the financial support of the Spanish MINECO-FEDER (Grants PID2020-116861GB–I00 and RED2018-102387-T). UAB is also acknowledged by a PIF grant to G.N., and Generalitat de Catalunya for grant 2017SGR1323. P. Vidossich is acknowledged for his helpful comments.

Conflict of Interest

The authors declare no conflict of interest.

Data Availability Statement

The data that support the findings of this study are available in the supplementary material of this article.

Keywords: density functional theory · metallocage · molecular dynamics · Nazarov cyclization · supramolecular catalysis

[1] A. J. McConnell, C. J. E. Haynes, C. Caltagirone, J. R. Hiscock, *ChemPlusChem* **2020**, *85*, 2544–2545.
[2] W. Liu, J. F. Stoddart, *Chem.* **2021**, *7*, 919–947.
[3] J. L. Atwood, *Comprehensive Supramolecular Chemistry II*; Elsevier, Amsterdam, **2017**.
[4] Y. Voloshin, I. Belaya, R. Krämer, *The Encapsulation Phenomenon: Synthesis, Reactivity and Applications of Caged Ions and Molecules*; Springer, Cham, **2016**.
[5] C. García-Simón, M. Garcia-Borràs, L. Gómez, T. Parella, S. Osuna, J. Juanhuix, I. Imaz, D. Maspoch, M. Costas, X. Ribas, *Nat. Commun.* **2014**, *5*, 5557.
[6] W. N. M. Van Leeuwen, M. Raynal, *Supramolecular Catalysis*; Wiley-VCH, Weinheim, **2008**.
[7] W. N. M. Van Leeuwen, M. Raynal, *Supramolecular Catalysis: New Directions and Developments*; Wiley-VCH, Weinheim, **2022**.
[8] M. Morimoto, S. M. Bierschenk, K. T. Xia, R. G. Bergman, K. N. Raymond, F. D. Toste, *Nat. Catal.* **2020**, *3*, 969–984.
[9] D. M. Vriezema, M. Comellas Aragonès, J. A. A. W. Elemans, J. J. L. M. Cornelissen, A. E. Rowan, R. J. M. Nolte, *Chem. Rev.* **2005**, *105*, 1445–1490.
[10] T. S. Koblenz, J. Wassenaar, J. N. H. Reek, *Chem. Soc. Rev.* **2008**, *37*, 247–262.
[11] M. Raynal, P. Ballester, A. Vidal-Ferran, P. W. N. M. van Leeuwen, *Chem. Soc. Rev.* **2014**, *43*, 1734–1787.
[12] S. H. A. M. Leenders, R. Gramage-Doria, B. de Bruin, J. N. H. Reek, *Chem. Soc. Rev.* **2015**, *44*, 433–448.
[13] H. Vardhan, F. Verpoort, *Adv. Synth. Catal.* **2015**, *357*, 1351–1368.
[14] D. L. Caulder, C. Brückner, R. E. Powers, S. König, T. N. Parac, J. A. Leary, K. N. Raymond, *J. Am. Chem. Soc.* **2001**, *123*, 8923–8938.
[15] M. Yoshizawa, M. Tamura, M. Fujita, *Science* **2006**, *312*, 251–254.
[16] J. L. Bolliger, A. M. Belenguer, J. R. Nitschke, *Angew. Chem. Int. Ed.* **2013**, *52*, 7958–7962; *Angew. Chem.* **2013**, *125*, 8116–8120.
[17] H. Amouri, C. Desmarets, J. Moussa, *Chem. Rev.* **2012**, *112*, 2015–2041.
[18] M. D. Pluth, R. G. Bergman, K. N. Raymond, *Science* **2007**, *316*, 85–88.
[19] D. M. Kaphan, M. D. Levin, R. G. Bergman, K. N. Raymond, F. D. Toste, *Science* **2015**, *350*, 1235–1238.
[20] M. D. Levin, D. M. Kaphan, C. M. Hong, R. G. Bergman, K. N. Raymond, F. D. Toste, *J. Am. Chem. Soc.* **2016**, *138*, 9682–9693.
[21] G. Norjmaa, J–D. Maréchal, G. Ujaque, *J. Am. Chem. Soc.* **2019**, *141*, 13114–13123.
[22] G. Norjmaa, J–D. Maréchal, G. Ujaque, *Chem. Eur. J.* **2020**, *26*, 6988–6992.
[23] G. Norjmaa, J–D. Maréchal, G. Ujaque, *Chem. Eur. J.* **2021**, *27*, 15973–15980.
[24] Z. J. Wang, C. J. Brown, R. G. Bergman, K. N. Raymond, F. D. Toste, *J. Am. Chem. Soc.* **2011**, *133*, 7358–7360.
[25] D. H. Leung, R. G. Bergman, K. N. Raymond, *J. Am. Chem. Soc.* **2007**, *129*, 2746–2747.
[26] C. J. Brown, R. G. Bergman, K. N. Raymond, *J. Am. Chem. Soc.* **2009**, *131*, 17530–17531.
[27] D. H. Leung, R. G. Bergman, K. N. Raymond, *J. Am. Chem. Soc.* **2006**, *128*, 9781–9797.
[28] C. M. Hong, R. G. Bergman, K. N. Raymond, F. D. Toste, *Acc. Chem. Res.* **2018**, *51*, 2447–2455.
[29] C. J. Hastings, M. D. Pluth, R. G. Bergman, K. N. Raymond, *J. Am. Chem. Soc.* **2010**, *132*, 6938–6940.
[30] A. Radzicka, R. Wolfenden, *Science.* **1995**, *267*, 90–93.
[31] C. J. Hastings, R. G. Bergman, K. N. Raymond, *Chem. Eur. J.* **2014**, *20*, 3966–3973.
[32] C. Goehry, M. Besora, F. Maseras, *ACS Catal.* **2015**, *5*, 2445–2451.
[33] Y. Ootani, Y. Akinaga, T. Nakajima, *J. Comput. Chem.* **2015**, *36*, 459–466.
[34] "*Catalysis by Metal–Organic Cages: A Computational Perspective*": G. Sciortino, G. Norjmaa, J–D. Maréchal, G. Ujaque in *Supramolecular Catalysis: New Directions and Developments*, Wiley-VCH, Weinheim **2022**; pp 271–285.
[35] C. Garciá-Simón, C. Colomban, Y. A. Çetin, A. Gimeno, M. Pujals, E. Ubasart, C. Fuertes-Espinosa, K. Asad, N. Chronakis, M. Costas, J. Jiménez-Barbero, F. Feixas, X. Ribas, *J. Am. Chem. Soc.* **2020**, *142*, 16051–16063.
[36] A. Tarzia, K. E. Jelfs, *Chem. Commun.* **2022**, *58*, 3717–3730.
[37] W–L. Li, H. Hao, T. Head-Gordon, *ACS Catal.* **2022**, *12*, 3782–3788.
[38] M. P. Frushicheva, S. Mukherjee, A. Warshel, *J. Phys. Chem. B* **2012**, *116*, 13353–13360.
[39] V. Vaissier Welborn, T. Head-Gordon, *J. Phys. Chem. Lett.* **2018**, *9*, 3814–3818.
[40] F. Sebastiani, T. A. Bender, S. Pezzotti, W. L. Li, G. Schwaab, R. G. Bergman, K. N. Raymond, F. D. Toste, T. Head-Gordon, M. Havenith, *Proc. Natl. Acad. Sci. USA* **2020**, *117*, 32954–32961.
[41] T. A. Young, V. Martí-Centelles, J. Wang, P. J. Lusby, F. Duarte, *J. Am. Chem. Soc.* **2020**, *142*, 1300–1310.
[42] H. Daver, J. N. Harvey, J. Rebek, F. Himo, *J. Am. Chem. Soc.* **2017**, *139*, 15494–15503.
[43] E. Pahima, Q. Zhang, K. Tiefenbacher, D. T. Major, *J. Am. Chem. Soc.* **2019**, *141*, 6234–6246.
[44] D. Chakraborty, P. K. Chattaraj, *J. Comput. Chem.* **2018**, *39*, 151–160.

[45] Q. N. N. Nguyen, K. T. Xia, Y. Zhang, N. Chen, M. Morimoto, X. Pei, Y. Ha, J. Guo, W. Yang, L–P. Wang, R. G. Bergman, K. N. Raymond, F. D. Toste, D. J. Tantillo, *J. Am. Chem. Soc.* **2022**, *144*, 11413–11424.
[46] J. R. Pliego, J. M. Riveros, *J. Phys. Chem. A.* **2002**, *106*, 7434–7439.
[47] M. A. Ortuño, A. Lledós, *J. Organomet. Chem.* **2021**, *949*, 121957.
[48] G. Norjmaa, P. Vidossich, J–D. Maréchal, G. Ujaque, *J. Chem. Inf. Model.* **2021**, *61*, 4370–4381.
[49] Gaussian09, Revision D.01,M. J. Frisch, G. W. Trucks, H. B. Schlegel, G. E. Scuseria, M. A. Robb, J. R. Cheeseman, G. Scalmani, V. Barone, B. Mennucci, G. A. Petersson, H. Nakatsuji, M. Caricato, X. Li, H. P. Hratchian, A. F. Izmaylov, J. Bloino, G. Zheng, J. L. Sonnenberg, M. Hada, M. Ehara, K. Toyota, R. Fukuda, J. Hasegawa, M. Ishida, T. Nakajima, Y. Honda, O. Kitao, H. Nakai, T. Vreven, J. A. Montgomery, Jr., J. E. Peralta, F. Ogliaro, M. Bearpark, J. J. Heyd, E. Brothers, K. N. Kudin, V. N. Staroverov, T. Keith, R. Kobayashi, J. Normand, K. Raghavachari, A. Rendell, J. C. Burant, S. S. Iyengar, J. Tomasi, M. Cossi, N. Rega, J. M. Millam, M. Klene, J. E. Knox, J. B. Cross, V. Bakken, C. Adamo, J. Jaramillo, R. Gomperts, R. E. Stratmann, O. Yazyev, A. J. Austin, R. Cammi, C. Pomelli, J. W. Ochterski, R. L. Martin, K. Morokuma, V. G. Zakrzewski, G. A. Voth, P. Salvador, J. J. Dannenberg, S. Dapprich, A. D. Daniels, O. Farkas, J. B. Foresman, J. V. Ortiz, J. Cioslowski, D. J. Fox, Gaussian, Inc., WallingfordCT, **2013**.
[50] A. D. Becke, *J. Chem. Phys.* **1993**, *98*, 5648–5652.
[51] C. Lee, W. Yang, R. G. Parr, *Phys. Rev. B: Condens. Matter Mater. Phys.* **1988**, *37*, 785–789.
[52] S. Grimme, J. Antony, S. Ehrlich, H. Krieg, *J. Chem. Phys.* **2010**, *132*, 154104–154119.
[53] T. H. Dunning, P. J. Hay, Modern Theoretical Chemistry; Schaefer, H. F., III, Eds.; Plenum: New York, **1977**; Vol. 3, pp 1–28.
[54] A. Höllwarth, M. Böhme, S. Dapprich, A. W. Ehlers, A. Gobbi, V. Jonas, K. F. Köhler, R. Stegmann, A. Veldkamp, G. Frenking, *Chem. Phys. Lett.* **1993**, *208*, 237–240.
[55] V. A. Rassolov, M. A. Ratner, J. A. Pople, P. C. Redfern, L. A. Curtiss, *J. Comput. Chem.* **2001**, *22*, 976–984.
[56] A. V. Marenich, C. J. Cramer, D. G. Truhlar, *J. Phys. Chem. B* **2009**, *113*, 6378–6396.
[57] S. Grimme, *Chem. Eur. J.* **2012**, *18*, 9955–9964.
[58] V. S. Bryantsev, M. S. Diallo, W. A. Goddard, *J. Phys. Chem. B* **2008**, *112*, 9709–9719.
[59] D. A. Case, R. M. Betz, D. S. Cerutti, T. E. Cheatham, III, T. A. Darden, R. E. Duke, T. J. Giese, H. Gohlke, A. W. Goetz, N. Homeyer, S. Izadi, P. Janowski, J. Kaus, A. Kovalenko, T. S. Lee, S. LeGrand, P. Li, C. Lin, T. Luchko, R. Luo, B. Madej, D. Mermelstein, K. M. Merz, G. Monard, H. Nguyen, H. T. Nguyen, I. Omelyan, A. Onufriev, D. R. Roe, A. Roitberg, C. Sagui, C. L. Simmerling, W. M. Botello-Smith, J. Swails, R. C. Walker, J.Wang, R. M. Wolf, X. Wu, L. Xiao, P. A. Kollman (**2016**), AMBER2016, University of California, San Francisco.
[60] P. Mark, L. Nilsson, *J. Phys. Chem. A* **2001**, *105*, 9954–9960.
[61] J. Yin, N. M. Henriksen, D. R. Slochower, M. K. Gilson, *J. Comput.-Aided Mol. Des.* **2017**, *31*, 133–145.
[62] J. Yin, N. M. Henriksen, D. R. Slochower, M. K. Gilson, AMBER Advanced Tutorial 29 Computing Binding Free Energy and Binding Enthalpy Using the Attach-Pull-Release (APR) Method Example. **2016**, https://ambermd.org/tutorials/advanced/tutorial29/.
[63] G. Heinzelmann, N. M. Henriksen, M. K. Gilson, *J. Chem. Theory Comput.* **2017**, *13*, 3260–3275.
[64] V. Babin, C. Roland, C. Sagui, *J. Chem. Phys.* **2008**, *128*, 134101.

Manuscript received: June 10, 2022
Accepted manuscript online: July 20, 2022
Version of record online: September 1, 2022